



Mechanical squeezing in an active-passive-coupled double-cavity optomechanical system via pump modulation

QI GUO,^{1,2,*}  XIAO-QIAO REN,^{1,2} CHENG-HUA BAI,³ YUCHI ZHANG,^{1,2} GANG LI,^{1,2}  AND TIANCAI ZHANG^{1,2,4}

¹State Key Laboratory of Quantum Optics and Quantum Optics Devices, Institute of Opto-Electronics, College of Physics and Electronic Engineering, Shanxi University, Taiyuan, Shanxi 030006, China

²Collaborative Innovation Center of Extreme Optics, Shanxi University, Taiyuan 030006, China

³Department of Physics, School of Science, North University of China, Taiyuan, Shanxi 030051, China

⁴tczhang@sxu.edu.cn

*qguo@sxu.edu.cn

Abstract: We focus on the generation of mechanical squeezing by using periodically amplitude-modulated laser to drive an active-passive-coupled double-cavity optomechanical system, where the coupled gain cavity and loss cavity can form into a parity-time (\mathcal{PT})-symmetry system. The numerical analysis of the system stability shows that the system is more likely to be stable in the unbroken- \mathcal{PT} -symmetry regime than in the broken- \mathcal{PT} -symmetry regime. The mechanical squeezing in the active-passive system exhibits stronger robustness against the thermal noise than that in the passive-passive system, and the so-called 3 dB limit can be broken in the resolved-sideband regime. Furthermore, it is also found that the mechanical squeezing obtained in the unbroken- \mathcal{PT} -symmetry region is stronger than that in the broken- \mathcal{PT} -symmetry region. This work may be meaningful for the quantum state engineering in the gain-loss quantum system that contributes to the study of \mathcal{PT} -symmetric physics in the quantum regime.

© 2022 Optica Publishing Group under the terms of the [Optica Open Access Publishing Agreement](#)

1. Introduction

Due to the rapid development of microfabrication and nanotechnology, cavity optomechanics has become an ideal platform for studying macroscopic quantum phenomena and quantum information processing, and many significant progresses relying on cavity optomechanics platform in both experiment and theory have been made. So far, ground-state cooling of single or multiple mechanical oscillators [1–4], quantum entanglement (including optomechanical entanglement and mechanical-mechanical entanglement) [5–14], mechanical squeezing [5–7,15–20], and macroscopic quantum superposition [21] have been deeply studied. Wherein the generation of mechanical squeezing has been a significantly important goal in both fundamental studies and numerous potential applications related to quantum computation, quantum communication, and high-precision metrology [22–25], etc. Various schemes [5–7,15–20] have been proposed to realize the mechanical squeezing, even strong mechanical squeezing, i.e., the steady-state squeezing by a factor of 1/2 below the zero-point level (the so-called 3 dB limit). Parallel to theoretical research, much progress has been made in experiment. For example, different experimental schemes for generating mechanical squeezing has been achieved in microwave optomechanical systems [26–28]. Especially, the mechanical squeezing of a micron-scale mechanical oscillator breaking the 3 dB limit has been observed by using the reservoir engineering technique based on two-tone driving [29].

On the other hand, non-Hermitian systems with \mathcal{PT} symmetry have attracted considerable attention since the pioneering work of Bender and Boettcher in 1998 [30]. If the Hamiltonian H of a system satisfies the commutation relation $[H, \hat{P}\hat{T}] = 0$ with the \mathcal{PT} operator $\hat{P}\hat{T}$, its

eigenvalues can be real. Moreover, a phase transition between the unbroken- \mathcal{PT} -symmetry and broken- \mathcal{PT} -symmetry will occur at the exceptional point (EP), where the eigenvalues and the corresponding eigenvectors coalesce and some novel physical phenomena may appear. Therefore, \mathcal{PT} -symmetry physics has become an active research area [31–35]. The experimental demonstrations of the \mathcal{PT} -symmetry and EP have been performed in various physical systems [36–39]. The engineering of EP has been extensively studied theoretically [40–45], and many amazing applications of \mathcal{PT} symmetry have been realized experimentally, such as unidirectional transmission [38,46], single-mode lasers [47,48], and enhanced sensitivity [49,50]. Particularly, Jing *et al.* combined \mathcal{PT} -symmetry physics and optomechanics to initiate the field of \mathcal{PT} optomechanics [51]. Based on \mathcal{PT} -symmetry optomechanics, various important phenomena have been predicted, such as phonon lasers [51–53], emergency of chaos at low-power threshold [54], enhanced ground-state cooling of mechanical oscillator [2,3,55], enhanced optomechanical entanglement [8], and so on.

Inspired by these works above, we here focus on the mechanical squeezing in the typical \mathcal{PT} -symmetric optomechanical system consisting of an active (gain) cavity to a passive (loss) optomechanical cavity driven by an amplitude-modulated laser field. The coupled-double-cavity system can form the \mathcal{PT} -symmetry structure. Firstly, the stability analysis of such system shows that the steady region are mostly located in the unbroken- \mathcal{PT} -symmetry regime. Then, it is found that the mechanical squeezing can be obtained, when a driving laser is blue-detuned, in both the unresolved-sideband and the resolved-sideband regime. Compared with the passive-passive double-cavity optomechanical system, the mechanical squeezing in the active-passive system is more robust against the mechanical thermal noise.

The rest of this paper is organized as follows. In Sec. 2, we describe the three-mode cavity optomechanical system and give the linearized Hamiltonian. In Sec. 3, we derive the dynamics of the system and analyze the stability of the system in the unresolved-sideband regime. Mechanical squeezing in both the unresolved-sideband and resolved-sideband regime are presented in Sec. 4. Finally, we conclude this work in Sec. 4.

2. Model and linearized Hamiltonian of the system

As schematically shown in Fig. 1, the three-mode system consists of an active optical cavity coupled to a passive cavity which is driven by an amplitude-modulated laser field with frequency ω_l and time-dependent amplitude $E(t)$. The amplitude of the external laser $E(t)$ is periodically modulated with the period τ ($E(t) = E(t + \tau)$). The active optical cavity is described by the bosonic annihilation (creation) operator a_1 (a_1^\dagger), whose frequency and gain are represented by ω_c and κ , respectively. a_2 (a_2^\dagger) is the annihilation (creation) operator of the passive cavity with frequency ω_c and decay rate γ , respectively. The cavity-cavity coupling strength is J . The mechanical resonator, with the resonance frequency ω_m and the decay rate γ_m , is described by the dimensionless position q and momentum p operators. g is the single-photon optomechanical coupling coefficient.

Therefore, the Hamiltonian of the whole system (in the unit of $\hbar = 1$) can be written as

$$H_1 = \omega_c a_1^\dagger a_1 + \omega_c a_2^\dagger a_2 + \frac{\omega_m}{2}(q^2 + p^2) - g a_2^\dagger a_2 q + J(a_1^\dagger a_2 + a_1 a_2^\dagger) + i[E(t)a_2^\dagger e^{-i\omega_l t} - E^*(t)a_2 e^{i\omega_l t}]. \quad (1)$$

In the frame rotating at the driving frequency ω_l , the Hamiltonian (1) becomes

$$H_2 = -\Delta a_1^\dagger a_1 - \Delta a_2^\dagger a_2 + \frac{\omega_m}{2}(q^2 + p^2) - g a_2^\dagger a_2 q + J(a_1^\dagger a_2 + a_1 a_2^\dagger) + i[E(t)a_2^\dagger - E^*(t)a_2]. \quad (2)$$

where $\Delta = \omega_l - \omega_c$ is the detuning of each cavity respecting to the driving laser.

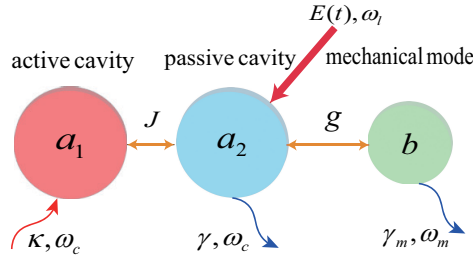


Fig. 1. Schematic diagram of the active-passive-coupled double-cavity optomechanics system. An active cavity (a_1) with gain rate κ is directly coupled to a passive cavity (a_2) with decay rate γ driven by an external laser with frequency ω_l and time-dependent amplitude $E(t)$. The frequencies of both cavities are ω_c . J is the cavity-cavity coupling strength. The mechanical oscillator (b) with frequency ω_m and decay rate γ_m is coupled to the passive cavity with optomechanical coupling strength g .

Taking mechanical damping, cavity decay (gain), and the environment noises into account, the dynamics of the system is completely described by the following nonlinear quantum Langevin equations (QLEs) [56]

$$\begin{aligned} \dot{q} &= \omega_m p, \\ \dot{p} &= -\omega_m q + g a_2^\dagger a_2 - \gamma_m p + \xi(t), \\ \dot{a}_1 &= (i\Delta + \kappa)a_1 - iJ a_2 + \sqrt{2\kappa} a_1^{\text{in}}(t), \\ \dot{a}_2 &= (i\Delta - \gamma)a_2 + i g a_2 q - iJ a_1 + E(t) + \sqrt{2\gamma} a_2^{\text{in}}(t). \end{aligned} \quad (3)$$

Here $a_1^{\text{in}}(t)$ and $a_2^{\text{in}}(t)$ are the corresponding zero-mean noise operators of two cavities with the nonzero correlation functions [56]

$$\begin{aligned} \langle a_j^{\text{in}}(t) a_j^{\text{in}\dagger}(t') \rangle &= (n_{aj} + 1) \delta(t - t'), \\ \langle a_j^{\text{in}\dagger}(t) a_j^{\text{in}}(t') \rangle &= n_{aj} \delta(t - t'), \end{aligned} \quad (4)$$

where $n_{aj} = [\exp(\hbar\omega_c/k_B T) - 1]^{-1}$ ($j = 1, 2$) is the mean bath photon number when the environmental temperature is T , and k_B is the Boltzmann constant. $\xi(t)$ is the zero-mean Brownian motion noise operator describing the dissipative friction forces acting on the mechanical oscillator, whose non-Markovian correlation function [57,58]

$$\langle \xi(t) \xi(t') \rangle = \frac{\gamma_m}{2\pi\omega_m} \int \left[\coth \left(\frac{\hbar\omega}{2k_B T} + 1 \right) \right] \omega e^{-i\omega(t-t')} d\omega. \quad (5)$$

For a mechanical oscillator with high quality factor $Q = \omega_m/\gamma_m \gg 1$, the above correlation function of $\xi(t)$ can be described by Markovian approximation as

$$\langle \xi(t) \xi(t') + \xi(t') \xi(t) \rangle / 2 \approx \gamma_m (2n_m + 1) \delta(t - t'), \quad (6)$$

where $n_m = [\exp(\hbar\omega_m/k_B T) - 1]^{-1}$ is the mean thermal phonon number.

Generally, it is difficult to solve the QLEs in Eq. (3) directly. Nevertheless, for the strong-driving regime, our physical model can be simplified by a linearization procedure. Then, we can rewrite each Heisenberg operator as the sum of the steady-state average and the quantum fluctuation: $O = \langle O \rangle + \delta O$ ($O = q, p, a_1, a_1^\dagger, a_2, a_2^\dagger$). Therefore, by replacing the Heisenberg operators in

Eq. (3) with the above summation form and applying the standard linearization technique, we can obtain the equations of motion for the classical first moments

$$\begin{aligned}
 \langle \dot{q}(t) \rangle &= \omega_m \langle p(t) \rangle, \\
 \langle \dot{p}(t) \rangle &= -\omega_m \langle q(t) \rangle + g |\langle a_2(t) \rangle|^2 - \gamma_m \langle p(t) \rangle, \\
 \langle \dot{a}_1(t) \rangle &= (i\Delta + \kappa) \langle a_1(t) \rangle - iJ \langle a_2(t) \rangle, \\
 \langle \dot{a}_2(t) \rangle &= (i\Delta - \gamma) \langle a_2(t) \rangle + ig \langle a_2(t) \rangle \langle q(t) \rangle - iJ \langle a_1(t) \rangle + E(t),
 \end{aligned}
 \tag{7}$$

and the linearized QLEs of the quantum fluctuation operator (hereafter we drop the notation δ for all the fluctuation operators for the sake of simplicity, like $\delta a_1 \rightarrow a_1$)

$$\begin{aligned}
 \frac{dq}{dt} &= \omega_m p, \\
 \frac{dp}{dt} &= -\omega_m q + g \langle a_2(t) \rangle^* a_2 + g \langle a_2(t) \rangle a_2^\dagger - \gamma_m p + \xi(t), \\
 \frac{da_1}{dt} &= (i\Delta + \kappa) a_1 - iJ a_2 + \sqrt{2\kappa} a_1^{\text{in}}(t), \\
 \frac{da_2}{dt} &= (i\Delta - \gamma) a_2 + ig \langle a_2(t) \rangle q + ig \langle q(t) \rangle a_2 - iJ a_1 + \sqrt{2\gamma} a_2^{\text{in}}(t).
 \end{aligned}
 \tag{8}$$

The linearized Hamiltonian corresponding to the linearized QLEs above reads

$$\begin{aligned}
 H_3 &= -\Delta a_1^\dagger a_1 - (\Delta + g \langle q(t) \rangle) a_2^\dagger a_2 + \frac{\omega_m}{2} (q^2 + p^2) \\
 &\quad + J(a_2^\dagger a_1 + a_2 a_1^\dagger) - g[\langle a_2(t) \rangle^* a_2 + \langle a_2(t) \rangle a_2^\dagger] q.
 \end{aligned}
 \tag{9}$$

In order to introduce the \mathcal{PT} -symmetric double-cavity structure clearly, we temporarily consider only the optical modes including the optical gain and loss and ignore the mechanical mode [38,39], then the non-Hermitian Hamiltonian can be written as

$$H_4 = (-\Delta + i\kappa) a_1^\dagger a_1 + (-\Delta - i\gamma) a_2^\dagger a_2 + J(a_2^\dagger a_1 + a_2 a_1^\dagger).
 \tag{10}$$

Obviously, for the cavities with the balanced gain and loss, the above Hamiltonian commutes with the \mathcal{PT} operator and is a \mathcal{PT} -symmetric Hamiltonian. In fact, the \mathcal{PT} symmetry can be generalized to the case where the gain rate κ and the decay rate γ is not exactly balanced. The complex eigenvalues of the above non-Hermitian Hamiltonian is

$$\omega_\pm = -\Delta - \frac{i(\gamma - \kappa)}{2} \pm \frac{\sqrt{4J^2 - (\gamma + \kappa)^2}}{2},
 \tag{11}$$

where the real and imaginary parts correspond to the eigenfrequencies and linewidths of the two supermodes, respectively. For a strong cavity-cavity coupling, i.e., $J > (\gamma + \kappa)/2$, the eigenvalues have two different real parts and an identical imaginary part, that is, the two supermodes have different frequencies $-\Delta \pm \sqrt{4J^2 - (\gamma + \kappa)^2}/2$ and an identical linewidth $(\gamma - \kappa)/2$, and the system is in the unbroken- \mathcal{PT} -symmetry regime. However, for the weak cavity-cavity coupling, i.e., $J < (\gamma + \kappa)/2$, the two supermodes coalesce and have the identical frequency and different linewidths, thus the system is in the broken- \mathcal{PT} -symmetry regime. The phase transition between the two regimes takes place around the critical point $J = (\gamma + \kappa)/2$ that is called an exceptional point (EP) corresponding to a spectral degeneracy of a non-Hermitian Hamiltonian.

3. Dynamics of the system and stability analysis

In order to generate the mechanical squeezing, it is very necessary to solve the dynamics of the quantum fluctuations in Eq. (8). To this end, we introduce the quadrature operators of the two

cavity modes and the corresponding input noise operators

$$\begin{aligned} X_j &= \frac{a_j + a_j^\dagger}{\sqrt{2}}, & Y_j &= \frac{a_j - a_j^\dagger}{i\sqrt{2}}, \\ X_j^{\text{in}} &= \frac{a_1^{\text{in}} + a_1^{\text{in}\dagger}}{\sqrt{2}}, & Y_j^{\text{in}} &= \frac{a_1^{\text{in}} - a_1^{\text{in}\dagger}}{i\sqrt{2}}, \end{aligned} \quad (12)$$

where $j = 1, 2$. We define the vector of the quadrature fluctuation operators and the vectors of corresponding noise operators

$$\begin{aligned} R(t) &= [q, p, X_1, Y_1, X_2, Y_2]^T, \\ N(t) &= [0, \xi(t), \sqrt{2\kappa_1}X_1^{\text{in}}(t), \sqrt{2\kappa_1}Y_1^{\text{in}}(t), \sqrt{2\kappa_2}X_2^{\text{in}}(t), \sqrt{2\kappa_2}Y_2^{\text{in}}(t)]^T. \end{aligned} \quad (13)$$

Then, the linearized QLEs in Eq. (8) governing the dynamics of the quantum fluctuations can be written in a compact form

$$\frac{dR}{dt} = A(t)R + N(t), \quad (14)$$

where $A(t)$ is a 6×6 time-dependent matrix

$$A(t) = \begin{bmatrix} 0 & \omega_m & 0 & 0 & 0 & 0 \\ -\omega_m & -\gamma_m & 0 & 0 & G_x(t) & G_y(t) \\ 0 & 0 & \kappa & -\Delta & 0 & J \\ 0 & 0 & \Delta & \kappa & -J & 0 \\ -G_y(t) & 0 & 0 & J & -\gamma & -\tilde{\Delta} \\ G_x(t) & 0 & -J & 0 & \tilde{\Delta} & -\gamma \end{bmatrix}, \quad (15)$$

in which $\tilde{\Delta} = \Delta + g\langle q(t) \rangle$; $G_x(t)$ and $G_y(t)$ are the real and imaginary parts of the effective coupling strength $G(t) = \sqrt{2}g\langle a_2(t) \rangle$, respectively. The formal solution of Eq. (13) is

$$R(t) = L(t)R(0) + L(t) \int_0^t L^{-1}(\tau)N(\tau)d\tau, \quad (16)$$

here $L(t) = \mathcal{T} \exp \left[\int_0^t A(\tau)d\tau \right] L(0)$ and \mathcal{T} represents the time-ordering operator.

Due to the linearized dynamics of the quantum fluctuations and the zero-mean Gaussian nature of the quantum noises, the time evolution of the quantum fluctuations can be completely described by the 6×6 covariance matrix (CM) $V(t)$ whose matrix element is defined as

$$V_{k,l} = \langle R_k(t)R_l(t) + R_l(t)R_k(t) \rangle / 2. \quad (17)$$

We can derive the motion equation of the CM $V(t)$ according to Eqs. (13), (15), and (16)

$$\frac{dV}{dt} = A(t)V(t) + V(t)A^T(t) + D \quad (18)$$

where $A^T(t)$ denotes the transpose of $A(t)$; the diffusion matrix D is

$$D = \text{diag}[0, \gamma_m(2n_m + 1), \kappa(2n_{a1} + 1), \kappa(2n_{a1} + 1), \gamma(2n_{a2} + 1), \gamma(2n_{a2} + 1)]. \quad (19)$$

The evolution equation of the CM $V(t)$ can completely described the dynamic evolution of quantum fluctuations and can be used to analyze the quantum properties of the system.

Because the amplitude of the driving laser is modulated very gently, in order to analyze the stability of the system over a larger range of driving amplitude, we here make driving laser independent of time, i.e. the first moment of the operators and the coefficient matrix in Eq. (15) are time-independent. According to the Routh-Hurwitz criterion [59], the system dynamics is stable if and only if all of the eigenvalues of the matrix A have negative real parts.

In Fig. 2, we show the effects of driving amplitude E , cavity-cavity coupling J , and gain-loss ratio κ/γ on the system stability, where yellow (blue) represents the stable (unstable) region and the optomechanical cavity is in the unresolved-sideband regime. Figures 2(a) and (b) display the system stability versus E and J for $\kappa = 0.01\gamma$ and $\kappa = 0.4\gamma$, respectively, in which the red dashed lines are composed of the EPs, i.e., $J = 0.505\gamma$ ($\kappa = 0.01\gamma$) and $J = 0.7\gamma$ ($\kappa = 0.4\gamma$). It can be found that the system stable region shrinks as the system moves towards the balanced gain and loss, and the stable region mainly locates in the unbroken- \mathcal{PT} -symmetry regime, i.e., before the two supermodes coalesce. Figures 2(c) and (d) exhibit the system stability versus E and κ/γ for $J=0.4\gamma$ and $J=\gamma$, respectively, from which we can see the stable region expands with the increase of coupling strength J . Therefore, the strong coupling J and low gain-loss ratio κ/γ are beneficial to the stability of the system. The coupling strength J in the unbroken- \mathcal{PT} -symmetry regime is larger than that in the broken- \mathcal{PT} -symmetry regime, so under the same conditions, the system is more likely to be stable in the unbroken- \mathcal{PT} -symmetry regime. In the following section, we will study the mechanical squeezing in these stable regions.

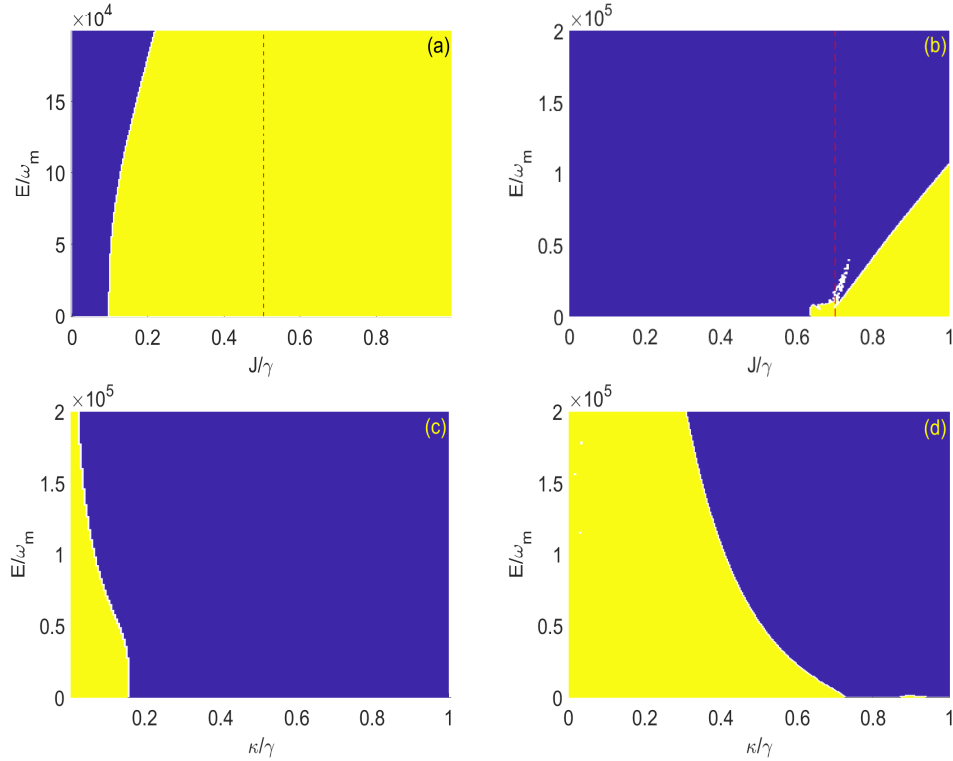


Fig. 2. Diagram of the system stability versus E and J for $\kappa = 0.01\gamma$ (a) and $\kappa = 0.4\gamma$ (b), the system stability versus E and κ/γ for $J = 0.4\gamma$ (c) and $J = \gamma$ (d). The yellow (blue) region represents the stable (unstable) region of the system. The red dashed lines in (a) and (b) indicate the EPs. The chosen system parameters are (in units of ω_m): $\Delta = 1$, $\gamma_m = 10^{-6}$, $g = 8 \times 10^{-5}$, $\gamma = 6.5$, and the thermal noises are absence ($n_m = n_a = 0$).

4. Mechanical squeezing in the unresolved-sideband and resolved-sideband regimes

When the conventional dissipative optomechanical cavity is driven by a periodically amplitude-modulated laser field, it has been demonstrated that the mechanical squeezing will be generated [5], and the passive-passive double cavities will enhance the mechanical squeezing [7]. Here we want to show what will happen in a periodically amplitude-modulated active-passive double-cavity optomechanical system. The periodically modulated amplitude $E(t)$ can be expanded by using Fourier series

$$E(t) = \sum_{n=-\infty}^{\infty} E_n e^{-in\Omega t} \quad (20)$$

where $\Omega = 2\pi/\tau$ is the fundamental modulation frequency and τ is the modulated period. For the following numerical analysis, we approximately truncate the series of the modulated amplitude to the first terms, i.e., the time-dependent amplitude takes the form of $E(t) = E_{-1}e^{i\Omega t} + E_0 + E_1e^{-i\Omega t}$. Substitute $E(t)$ into Eq. (7), then we can numerically solve the motion equation of the CM $V(t)$ to study the quantum behaviors of the system. As we all know, as long as the position variance $V(q)$ or the momentum variance $V(p)$ of the mechanical mode, i.e., the first or second diagonal elements of the CM $V(t)$, is less than $1/2$, we can come to conclusion that mechanical squeezing has been generated. Now we show the generation of mechanical squeezing in the unresolved-sideband ($\gamma > \omega_m$) regime by numerically evaluating the position variance $V(q)$ in Fig. 3, where the system parameters are chosen according to the stable region in Fig. 2. $J = 0.6\gamma$, $E_0 = 1.4 \times 10^5 \omega_m$, and $E_{\pm 1} = 3 \times 10^4 \omega_m$. The modulation frequency is chosen as $\Omega = 2\omega_m$, following the result of Ref. [5], whose physical mechanism can be understood by analogy with the parametric amplification: the variation of the spring constant of the mechanical motion in time with just twice the frequency of the mechanical motion will leads to the squeezing of the mechanical mode. The other parameters are the same as those in Fig. 2(a).

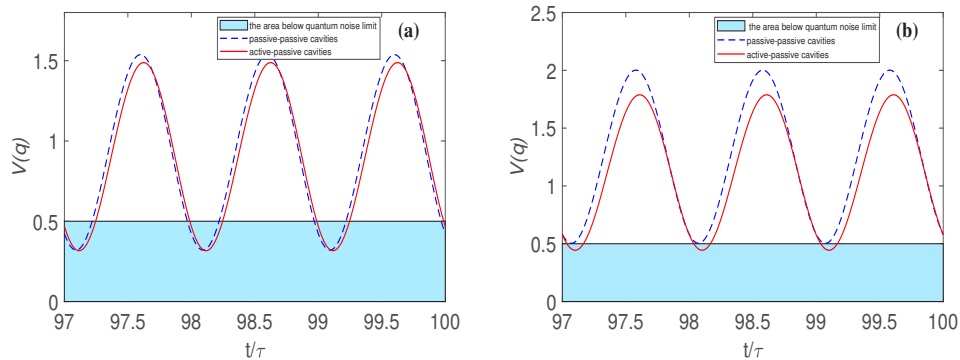


Fig. 3. Time evolution of the mechanical position operator variance in the unresolved-sideband regime for the mean thermal phonon number (a) $n_m = 0$ and (b) $n_m = 6000$. The red solid (blue dashed) line represents the position variance in the active-passive (passive-passive) cavity optomechanical system. The rectangular light blue areas (shadow areas) represent the region below quantum noise limit. The chosen parameters are $J = 0.6\gamma$, $E_0 = 1.4 \times 10^5 \omega_m$, $E_{\pm 1} = 3 \times 10^4 \omega_m$, and $\Omega = 2\omega_m$. The other parameters are the same as those in Fig. 2(a).

The system driven by a periodically amplitude-modulated laser field will reach steady state after a long period of time. In Fig. 3, we plot $V(q)$ versus the time from $t = 97\tau$ to $t = 100\tau$. The red solid line in Fig. 3 represents the position variance $V(q)$ in the active-passive cavity optomechanical system, while the blue dashed line represents the $V(q)$ in the passive-passive

cavity optomechanical system, which can be achieved by choosing the negative value of the gain κ . The periodic oscillation of the variance $V(q)$ over time indicates that the squeezing direction changes periodically, and the change period is the same as the modulation period. Figures 3(a) and (b) correspond to the cases the mechanical thermal phonon number $n_m = 0$ and $n_m = 12000$, respectively. From Fig. 3(a), we can see the mechanical squeezing can be generated in both the active-passive and passive-passive system, the squeezing in the active-passive system is slightly better than that in the passive-passive system. For example, the the minimum $V(q)$ in the active-passive system is 0.3166, and in the passive-passive system is 0.3205. That is, the active-passive system seems to have little advantage over the passive-passive system. However, when the thermal noise is taken into account and the mean thermal phonon number $n_m = 12000$ as shown in Fig. 3(b), the squeezing in the active-passive system can still be generated, while the mechanical mode cannot be squeezed in the passive-passive system. That is, the active-passive-coupled system has stronger robustness against the thermal noise than the passive-passive-coupled system. The physics behind the results above can be understood as follows. On the one hand, the mechanical squeezing is generated through the nonlinearity induced by the periodically amplitude-modulated pump [5] rather than the gain of the active cavity, so when the thermal noise is not taken into account, the mechanical squeezing in the active-passive-coupled system is almost no better than that in the passive-passive-coupled system. On the other hand, the coupled system can be regarded as a whole, and the gain of the active cavity can balance a part of the dissipation of the passive cavity. Therefore, the overall dissipation of the active-passive system is essentially less than that of the passive-passive system, and thus the active-passive system will have stronger robustness against the thermal noise than the passive-passive system according to the fluctuation-dissipation theorem.

The mechanical squeezing can be generated in the unresolved-sideband regime, but the strong squeezing breaking the so-called 3 dB limit cannot achieved. Now we numerically evaluate the position variance $V(q)$ in the resolved-sideband regime, as shown in Fig. 4, where the red solid (blue dashed) line represents the position variance for the mean thermal phonon number $n_m = 0$ ($n_m = 1000$), and the loss of the optomechanical cavity $\gamma = 0.2\omega_m$. We can see the 3 dB limit of the mechanical squeezing based on the parametric interaction can be broken ($V(q) < 0.25$) in the resolved-sideband regime. The minimum variance $V(q) = 0.1469$ for $n_m = 0$. The strong mechanical squeezing can be still achieved even in the presence of thermal noise (the minimum $V(q) = 0.2386$ for $n_m = 1000$), which once again proves the mechanical squeezing scheme in the active-passive-coupled system has strong robustness against the thermal noise. What we want to point out is that, although the mechanical squeezing here is slightly increased and has stronger robustness against the thermal noise than that in the passive-passive-coupled system, the present scheme requires the introduction of gain to a cavity, which will inevitably increase the difficulty of the experiment. Fortunately, the active cavity has been fabricated from Er^{3+} -doped silica and can emit photons in the 1550-nm band by optically pumping Er^{3+} ions with a pump laser in the 1460-nm band [38], which ensures the experimental feasibility of the present scheme.

To compare the mechanical squeezing before and after the two supermodes coalesce, we plot the evolution of single-mode squeezing parameter r over time in Fig. 5 for different cavity-cavity coupling strengths J , where the squeezing parameter r is defined as the logarithm of the minimum eigenvalue of the CM $V(t)$ [5]. The system parameters are the same as those in Fig. 2(a). From Fig. 5, we can see the steady-state squeezing parameter increases with the increase of J . $J = 0.505$ corresponds to the EP (the red dashed line in Fig. 2(a)), and $J > 0.505$ ($J < 0.505$) corresponds to the unbroken- \mathcal{PT} -symmetry (broken- \mathcal{PT} -symmetry) regime, i.e., before (after) the two supermodes coalesce. Therefore, Fig. 5 shows the mechanical squeezing in the unbroken- \mathcal{PT} -symmetry regime is stronger than that in the broken- \mathcal{PT} -symmetry regime.

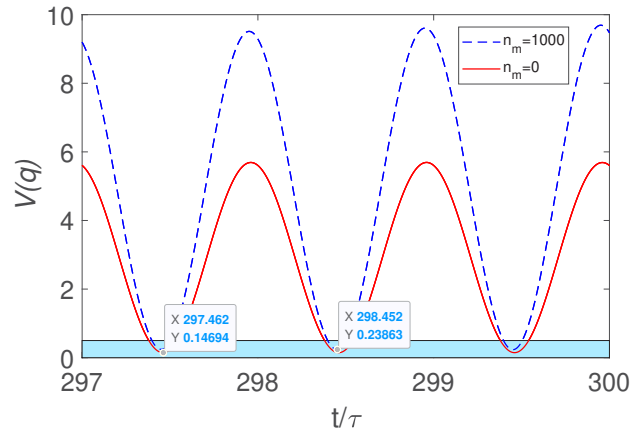


Fig. 4. Time evolution of the mechanical position operator variance in the resolved-sideband regime. The red solid and blue dashed lines represent the cases that the mean thermal phonon number $n_m = 0$ and $n_m = 1000$, respectively. The rectangular blue area (shadow area) represents the region below quantum noise limit. The chosen system parameters are $\gamma = 0.2\omega_m$, $\kappa = 0.1\gamma$, $J = 12\gamma$, $E_0 = 1.4 \times 10^5 \omega_m$, $E_{\pm 1} = 2 \times 10^4 \omega_m$. The other parameters are the same as those in Fig. 3.

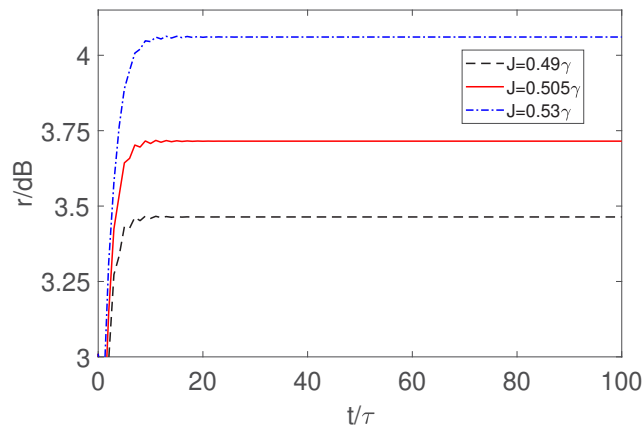


Fig. 5. Time evolution of the mechanical mode-squeezing parameter r for different cavity-cavity coupling strengths J . The chosen parameters are the same as those in Fig. 2(a).

5. Conclusions

In conclusion, we have investigated the mechanical squeezing in an active-passive-coupled double-cavity optomechanics system driven by a periodically amplitude-modulated laser. The coupled loss and gain cavities can form into a \mathcal{PT} -symmetry system. We derived dynamics of the active-passive optomechanics system, and further analyzed its stability, which shows that the system is generally unstable in the broken- \mathcal{PT} -symmetry regime, while more stable in the unbroken- \mathcal{PT} -symmetry regime. We found that when the driving laser is blue-detuned respecting to the cavity frequency, the mechanical squeezing can be generated in both the resolved-sideband regime and the unresolved-sideband regime. What's more, the strong mechanical squeezing can be achieved in the resolved-sideband regime even when the thermal noise is present. Compared with the passive-passive-coupled double-cavity optomechanics system, we have shown the mechanical squeezing in the active-passive system is more robust against the mechanical thermal noise. It is also demonstrated that the degree of the mechanical squeezing in the unbroken- \mathcal{PT} -symmetry regime is higher than that in the broken- \mathcal{PT} -symmetry regime. What's more, the active-passive-coupled double-cavity system has been realized experimentally that makes the presented scheme feasible in experiment. Therefore, this work can not only provide an effective quantum resource for quantum information and quantum precision measurement based on cavity optomechanics, but also may be meaningful for the study of \mathcal{PT} -symmetric physics in the quantum regime.

Funding. National Natural Science Foundation of China (12274274, 11604190, 11974223, U21A20433, U21A6006); National Key Research and Development Program of China (2021YFA1402002).

Disclosures. The authors declare no conflicts of interest.

Data availability. Data underlying the results presented in this paper are not publicly available at this time but may be obtained from the authors upon reasonable request.

References

1. Y.-J. Guo, K. Li, W.-J. Nie, and Y. Li, "Electromagnetically-induced-transparency-like ground-state cooling in a double-cavity optomechanical system," *Phys. Rev. A* **90**(5), 053841 (2014).
2. Y.-L. Liu and Y.-x. Liu, "Energy localization enhanced ground-state cooling of mechanical resonator from room temperature in optomechanics using a gain cavity," *Phys. Rev. A* **96**(2), 023812 (2017).
3. H. Jing, Ş. K. Özdemir, H. Lü, and F. Nori, "High-order exceptional points in optomechanics," *Sci. Rep.* **7**(1), 3386 (2017).
4. C.-H. Bai, D.-Y. Wang, S. Zhang, S.-T. Liu, and H.-F. Wang, "Double-mechanical-oscillator cooling by breaking the restrictions of quantum backaction and frequency ratio via dynamical modulation," *Phys. Rev. A* **103**(3), 033508 (2021).
5. A. Mari and J. Eisert, "Gently modulating optomechanical systems," *Phys. Rev. Lett.* **103**(21), 213603 (2009).
6. C.-H. Bai, D.-Y. Wang, S. Zhang, S.-T. Liu, and H.-F. Wang, "Modulation-based atom-mirror entanglement and mechanical squeezing in an unresolved-sideband optomechanical system," *Ann. Phys.* **531**(7), 1800271 (2019).
7. W.-J. Zhang, Y.-C. Zhang, Q. Guo, A.-P. Liu, G. Li, and T.-C. Zhang, "Strong mechanical squeezing and optomechanical entanglement in a dissipative double-cavity system via pump modulation," *Phys. Rev. A* **104**(5), 053506 (2021).
8. C. Tchodimou, P. Djorwe, and S. G. Nana Engo, "Distant entanglement enhanced in \mathcal{PT} -symmetric optomechanics," *Phys. Rev. A* **96**(3), 033856 (2017).
9. Y.-D. Wang and A. A. Clerk, "Reservoir-engineered entanglement in optomechanical systems," *Phys. Rev. Lett.* **110**(25), 253601 (2013).
10. D. Vitali, S. Gigan, A. Ferreira, H. R. Böhm, P. Tombesi, A. Guerreiro, V. Vedral, A. Zeilinger, and M. Aspelmeyer, "Optomechanical entanglement between a movable mirror and a cavity field," *Phys. Rev. Lett.* **98**(3), 030405 (2007).
11. X. Y. Huang, E. Zeuthen, D. V. Vasilyev, Q. Y. He, K. Hammerer, and E. S. Polzik, "Unconditional steady-State entanglement in macroscopic hybrid systems by coherent noise cancellation," *Phys. Rev. Lett.* **121**(10), 103602 (2018).
12. M. Wang, X. Y. Lü, Y. D. Wang, J. Q. You, and Y. Wu, "Macroscopic quantum entanglement in modulated optomechanics," *Phys. Rev. A* **94**(5), 053807 (2016).
13. Q. Lin, B. He, and M. Xiao, "Entangling two macroscopic mechanical resonators at high temperature," *Phys. Rev. Appl.* **13**(3), 034030 (2020).
14. C. F. Ockeloen-Korppi, E. Damskägg, J. M. Pirkkalainen, M. Asjad, A. A. Clerk, F. Massel, M. J. Woolley, and M. A. Sillanpää, "Stabilized entanglement of massive mechanical oscillators," *Nature (London)* **556**(7702), 478–482 (2018).

15. J.-Q. Liao and C. K. Law, "Parametric generation of quadrature squeezing of mirrors in cavity optomechanics," *Phys. Rev. A: At., Mol., Opt. Phys.* **83**(3), 033820 (2011).
16. X.-Y. Liao, J.-Q. Liao, L. Tian, and F. Nori, "Steady-state mechanical squeezing in an optomechanical system via duffing nonlinearity," *Phys. Rev. A* **91**(1), 013834 (2015).
17. W.-J. Gu, G.-X. Li, and Y.-P. Yang, "Generation of squeezed states in a movable mirror via dissipative optomechanical coupling," *Phys. Rev. A* **88**(1), 013835 (2013).
18. M. Asjad, G. S. Agarwal, M. S. Kim, P. Tombesi, G. Di Giuseppe, and D. Vitali, "Robust stationary mechanical squeezing in a kicked quadratic optomechanical system," *Phys. Rev. A* **89**(2), 023849 (2014).
19. D.-Y. Wang, C.-H. Bai, H.-F. Wang, A.-D. Zhu, and S. Zhang, "Steady-state mechanical squeezing in a hybrid atom-optomechanical system with a highly dissipative cavity," *Sci. Rep.* **6**(1), 24421 (2016).
20. D.-Y. Wang, C.-H. Bai, H.-F. Wang, A.-D. Zhu, and S. Zhang, "Steady-state mechanical squeezing in a double-cavity optomechanical system," *Sci. Rep.* **6**(1), 38559 (2016).
21. J.-Q. Liao and L. Tian, "Macroscopic quantum superposition in cavity optomechanics," *Phys. Rev. Lett.* **116**(16), 163602 (2016).
22. M. Aspelmeyer, T. J. Kippenberg, and F. Marquardt, "Cavity optomechanics," *Rev. Mod. Phys.* **86**(4), 1391–1452 (2014).
23. S. Mancini, D. Vitali, and P. Tombesi, "Scheme for teleportation of quantum states onto a mechanical resonator," *Phys. Rev. Lett.* **90**(13), 137901 (2003).
24. S. L. Braunstein and P. van Loock, "Quantum information with continuous variables," *Rev. Mod. Phys.* **77**(2), 513–577 (2005).
25. S. G. Hofer, W. Wicczorek, M. Aspelmeyer, and K. Hammerer, "Quantum entanglement and teleportation in pulsed cavity optomechanics," *Phys. Rev. A: At., Mol., Opt. Phys.* **84**(5), 052327 (2011).
26. E. E. Wollman, C. U. Lei, A. J. Weinstein, J. Suh, A. Kronwald, F. Marquardt, A. A. Clerk, and K. C. Schwab, "Quantum squeezing of motion in a mechanical resonator," *Science* **349**(6251), 952–955 (2015).
27. J.-M. Pirkkalainen, E. Damskägg, M. Brandt, F. Massel, and M. A. Sillanpää, "Squeezing of Quantum Noise of Motion in a Micromechanical Resonator," *Phys. Rev. Lett.* **115**(24), 243601 (2015).
28. F. Lecocq, J. B. Clark, R. W. Simmonds, J. Aumentado, and J. D. Teufel, "Quantum Nondemolition Measurement of a Nonclassical State of a Massive Object," *Phys. Rev. X* **5**(4), 041037 (2015).
29. C. U. Lei, A. J. Weinstein, J. Suh, E. E. Wollman, A. Kronwald, F. Marquardt, A. A. Clerk, and K. C. Schwab, "Quantum Nondemolition Measurement of a Quantum Squeezed State Beyond the 3 dB Limit," *Phys. Rev. Lett.* **117**(10), 100801 (2016).
30. C. M. Bender and S. Boettcher, "Real spectra in non-Hermitian Hamiltonians having \mathcal{PT} symmetry," *Phys. Rev. Lett.* **80**(24), 5243–5246 (1998).
31. Ş. K. Özdemir, S. Rotter, F. Nori, and L. Yang, "Parity-time symmetry and exceptional points in photonics," *Nat. Mater.* **18**(8), 783–798 (2019).
32. R. El-Ganainy, K. G. Makris, M. Khajavikhan, Z. H. Musslimani, S. Rotter, and D. N. Christodoulides, "Non-Hermitian Physics and PT Symmetry," *Nat. Phys.* **14**(1), 11–19 (2018).
33. M.-A. Miri and A. Alù, "Exceptional points in optics and photonics," *Science* **363**(6422), eaar7709 (2019).
34. V. V. Konotop, J. Yang, and D. A. Zezyulin, "Nonlinear waves in \mathcal{PT} -symmetric systems," *Rev. Mod. Phys.* **88**(3), 035002 (2016).
35. L. Feng, R. El-Ganainy, and L. Ge, "Non-Hermitian photonics based on parity-time symmetry," *Nat. Photonics* **11**(12), 752–762 (2017).
36. S. Klaiman, U. Günther, and N. Moiseyev, "Visualization of Branch Points in PT-Symmetric Waveguides," *Phys. Rev. Lett.* **101**(8), 080402 (2008).
37. A. Guo, G. J. Salamo, D. Duchesne, R. Morandotti, M. Volatier-Ravat, V. Aimez, G. A. Siviloglou, and D. N. Christodoulides, "Observation of PT-Symmetry Breaking in Complex Optical Potentials," *Phys. Rev. Lett.* **103**(9), 093902 (2009).
38. B. Peng, Ş. K. Özdemir, F. Lei, F. Monifi, M. Gianfreda, G. L. Long, S. Fan, F. Nori, C. M. Bender, and L. Yang, "Parity time-symmetric whispering-gallery microcavities," *Nat. Phys.* **10**(5), 394–398 (2014).
39. B. Peng, Ş. K. Özdemir, S. Rotter, H. Yilmaz, M. Liertzer, F. Monifi, C. M. Bender, F. Nori, and L. Yang, "Loss-induced suppression and revival of lasing," *Science* **346**(6207), 328–332 (2014).
40. F. Minganti, A. Miranowicz, R. W. Chhajlany, and F. Nori, "Quantum exceptional points of non-Hermitian Hamiltonians and Liouvillians: The effects of quantum jumps," *Phys. Rev. A* **100**(6), 062131 (2019).
41. P. C. Kuo, N. Lambert, A. Miranowicz, H. B. Chen, G. Y. Chen, Y. N. Chen, and F. Nori, "Collectively induced exceptional points of quantum emitters coupled to nanoparticle surface plasmons," *Phys. Rev. A* **101**(1), 013814 (2020).
42. F. Minganti, A. Miranowicz, R. W. Chhajlany, I. I. Arkhipov, and F. Nori, "Hybrid-Liouvillian formalism connecting exceptional points of non-Hermitian Hamiltonians and Liouvillians via postselection of quantum trajectories," *Phys. Rev. A* **101**(6), 062112 (2020).
43. I. I. Arkhipov, A. Miranowicz, F. Minganti, and F. Nori, "Liouvillian exceptional points of any order in dissipative linear bosonic systems: Coherence functions and switching between PT and anti-PT symmetries," *Phys. Rev. A* **102**(3), 033715 (2020).

44. I. I. Arkhipov, A. Miranowicz, F. Minganti, and F. Nori, "Quantum and semiclassical exceptional points of a linear system of coupled cavities with losses and gain within the Scully-Lamb laser theory," *Phys. Rev. A* **101**(1), 013812 (2020).
45. T.-X. Lu, H. Zhang, Q. Zhang, and H. Jing, "Exceptional-point-engineered cavity magnomechanics," *Phys. Rev. A* **103**(6), 063708 (2021).
46. L. Chang, X. Jiang, S. Hua, C. Yang, J. Wen, L. Jiang, G. Li, G. Wang, and M. Xiao, "Parity-time symmetry and variable optical isolation in active-passive-coupled microresonators," *Nat. Photonics* **8**(7), 524–529 (2014).
47. L. Feng, Z. J. Wong, R.-M. Ma, Y. Wang, and X. Zhang, "Singlemode laser by parity-time symmetry breaking," *Science* **346**(6212), 972–975 (2014).
48. H. Hodaei, M.-A. Miri, M. Heinrich, D. N. Christodoulides, and M. Khajavikhan, "Parity-time-symmetric microring lasers," *Science* **346**(6212), 975–978 (2014).
49. H. Hodaei, A. U. Hassan, S. Wittek, H. G.-Gracia, R. E.-Ganainy, D. N. Christodoulides, and M. Khajavikhan, "Enhanced sensitivity at higher-order exceptional points," *Nature* **548**(7666), 187–191 (2017).
50. W. Chen, Ş. K. Özdemir, G. Zhao, J. Wiersig, and L. Yang, "Exceptional points enhance sensing in an optical microcavity," *Nature* **548**(7666), 192–196 (2017).
51. H. Jing, Ş. K. Özdemir, X.-Y. Lü, J. Zhang, L. Yang, and F. Nori, "PT-symmetric phonon laser," *Phys. Rev. Lett.* **113**(5), 053604 (2014).
52. H. Lü, Ş. K. Özdemir, L. M. Kuang, F. Nori, and H. Jing, "Exceptional Points in Random-Defect Phonon Lasers," *Phys. Rev. Appl.* **8**(4), 044020 (2017).
53. J. Zhang, B. Peng, Ş. K. Özdemir, K. Pichler, D. O. Krimer, G. Zhao, F. Nori, Y. X. Liu, S. Rotter, and L. Yang, "A phonon laser operating at an exceptional point," *Nat. Photonics* **12**(8), 479–484 (2018).
54. X.-Y. Lü, H. Jing, J.-Y. Ma, and Y. Wu, "PT-symmetry-breaking chaos in optomechanics," *Phys. Rev. Lett.* **114**(25), 253601 (2015).
55. C. Jiang, Y.-L. Liu, and M.-A. Sillanpää, "Energy-level-attraction and heating-resistant-cooling of mechanical resonators with exceptional points," *Phys. Rev. A* **104**(1), 013502 (2021).
56. C. W. Gardiner and P. Zoller, *Quantum Noise*, 3rd ed. (Springer, New York, 2004).
57. V. Giovannetti and D. Vitali, "Phase-noise measurement in a cavity with a movable mirror undergoing quantum Brownian motion," *Phys. Rev. A* **63**(2), 023812 (2001).
58. A. A. Clerk, M. H. Devoret, S. M. Girvin, F. Marquardt, and R. J. Schoelkopf, "Introduction to quantum noise, measurement, and amplification," *Rev. Mod. Phys.* **82**(2), 1155–1208 (2010).
59. E. X. DeJesus and C. Kaufman, "Routh-Hurwitz criterion in the examination of eigenvalues of a system of nonlinear ordinary differential equations," *Phys. Rev. A* **35**(12), 5288–5290 (1987).